Nonlinear circuit quantum electrodynamics based on the charge-qubit–resonator interface

Deshui Yu,[1] Leong Chuan Kwek,[1,2,3,4] Luigi Amico,[1,5,6] and Rainer Dumke[1,7]
[1]*Centre for Quantum Technologies, National University of Singapore, 3 Science Drive 2, 117543 Singapore*
[2]*Institute of Advanced Studies, Nanyang Technological University, 60 Nanyang View, 639673 Singapore*
[3]*National Institute of Education, Nanyang Technological University, 1 Nanyang Walk, 637616 Singapore*
[4]*MajuLab, CNRS-UNS-NUS-NTU International Joint Research Unit, UMI 3654, Singapore*
[5]*CNR-MATIS-IMM and Dipartimento di Fisica e Astronomia, Universitá Catania, Via S. Soa 64, 95127 Catania, Italy*
[6]*INFN Laboratori Nazionali del Sud, Via Santa Sofia 62, I-95123 Catania, Italy*
[7]*Division of Physics and Applied Physics, Nanyang Technological University, 21 Nanyang Link, 637371 Singapore*

(Received 13 June 2018; published 28 September 2018)

We theoretically explore the applications of a nonlinear circuit QED system, where a charge qubit is inductively coupled to an LC resonator, in the photonic engineering and ultrastrong-coupling multiphoton quantum optics. An arbitrary Fock-state pulsed maser, where the artificial qubit plays the gain-medium role, is achieved via simply sweeping the gate-voltage bias. The resonantly pumped parametric qubit-resonator interface leads to a squeezed intraresonator field, which is utilizable for the quantum-limited microwave amplification. Moreover, upwards and downwards multiphoton quantum jumps may be observed in the driving-free steady-state system.

DOI: 10.1103/PhysRevA.98.033833

I. INTRODUCTION

Owing to properties of rapid operation, flexibility, and scalability, superconducting quantum circuits have become the most promising candidate for realizing quantum computation [1]. However, current practical execution is significantly limited by their short energy-relaxation and dephasing times (tens of microseconds [2]). Feedback control may persist the Rabi oscillation of superconducting qubits infinitely [3] and efficiently suppresses the low-frequency $1/f$ fluctuation in circuits [4,5]. In addition, hybrid schemes composed of superconducting circuits and neutral atoms potentially implement the quantum-state transfer between a rapid quantum processor and long-term memory [6–10].

Superconducting circuits also provide a vivid platform for exploring the fundamental principles of the matter-light interaction, especially in the ultrastrong-coupling regime which the conventional cavity quantum electrodynamics (QED) system barely accesses [11–13]. Multiple unique features have been recognized for the circuit QED [14]. Superconducting microwave resonators possess a quality factor much larger than high-finesse optical cavities [15], resulting in a longer lifetime of intraresonator photons. The capacitive or inductive coupling between artificial atoms and a resonator or between two arbitrary superconducting qubits in a many-body system may be designed deliberately and adjusted simply via tuning external voltage, current, or flux biases [16], leading to flexible and engineerable networks [17]. Moreover, the nonlinear dispersive artificial-atom–resonator interaction overcomes the weak-response obstacle in the quantum measurement and efficiently enhances the readout fidelity [18,19].

In this work, we theoretically investigate the potential applications of a circuit-QED structure, where a charge qubit nonlinearly interacts with a resonator, in aspects of preparing the photon-number-state microwave light, squeezing radiation, and quantum jump process. We find that an arbitrary Fock-state intraresonator field may be produced with a high fidelity by simply sweeping gate-charge and external flux biases. The resonant two-photon qubit-resonator coupling leads to the generation of squeezed radiation, which may be applied to suppress the quantum fluctuation in measurement. In addition, multiphoton quantum jumps are identified in the steady-state system. This nonlinear circuit QED paves the way for studying multiphoton quantum optics and quantum-state engineering [20].

II. PHYSICAL MODEL

We consider the nonlinear interface between a Cooper-pair box and an LC resonator as shown in Fig. 1(a). The box, which is biased by a voltage source V_g via a gate capacitor $C_g = 300$ aF, is connected to the Cooper-pair reservoir through two quasi-identical Josephson junctions with self-capacitances $C_j = 50$ aF and Josephson energy $\frac{E_J}{2\hbar} = 2\pi \times 10$ GHz. The tunneling rate of Cooper pairs between the box and the reservoir is tuned by an external flux Φ_{ex} [21]. The Cooper-pair box is characterized by the charge-number operator $\hat{N}$ and the net phase difference $\hat{\delta}$ across the Josephson junctions with the commutator of $[\hat{\delta}, \hat{N}] = i$. The microwave LC resonator consists of an inductor $L = 100$ nH and a capacitor $C = 500$ aF, resulting in the oscillation frequency $\omega_0 = (LC)^{-1/2} = 2\pi \times 22.5$ GHz. We use the operators $\hat{\phi}$ and $\hat{Q}$ to denote respectively the magnetic flux through L and the charge on C and have the commutator $[\hat{\phi}, \hat{Q}] = i\hbar$. A portion of $\hat{\phi}$, measured by $\xi \leqslant 1$, threads through the Cooper-pair-box loop, leading to the nonlinear inductive intercomponent coupling. The parameter ξ depends on the specific constructions of the Cooper-pair-box loop and the inductor

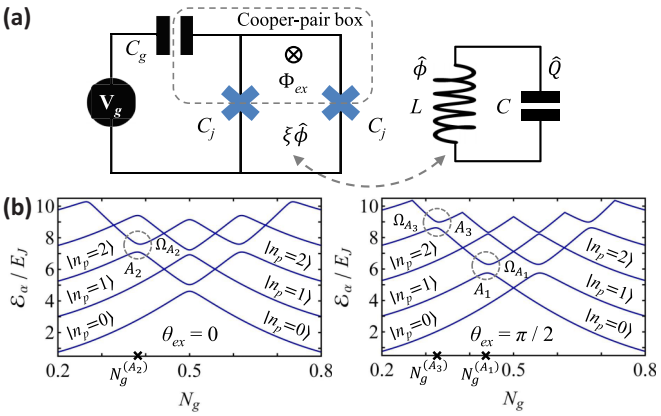

FIG. 1. (a) Schematics of nonlinear charge-qubit-resonator interface. The charge qubit is composed of a pair of Josephson junctions with the self-capacitance C_j. A voltage source V_g biases the Cooper-pair box via a gate capacitor C_g. An external flux Φ_{ex} is applied to tune the Josephson energy E_J of Cooper pairs. The LC resonator consists of an inductor L and a capacitor C. A flux portion from L, i.e., $\xi\hat{\phi}$, threads the Cooper-pair-box loop, leading to the nonlinear inductive qubit-resonator coupling. (b) Dependence of energy spectrum $\mathcal{E}_{\alpha=1,\ldots,5}$ on N_g with $\xi = 1$. Three anticrossings, which are shown in circles and labeled by $A_{i=1,2,3}$, occur at $N_g^{(A_{i=1,2,3})}$. The corresponding energy gaps are $\hbar\Omega_{A_{i=1,2,3}}$.

L as well as their relative position. In principle, ξ is tunable between zero and 1 (see the Appendix). The circuit operates at the temperature $T = 20$ mK with the thermal fluctuation $2\pi \times 0.4$ GHz.

The coherent Cooper-pair-box–resonator interplay is governed by the Hamiltonian

$$\hat{H} = E_C(\hat{N} - N_g)^2 + \hbar\omega_0\hat{a}^\dagger\hat{a} - E_J\cos[\theta_{ex} + \theta_L(\hat{a}^\dagger + \hat{a})]\cos\hat{\delta}, \tag{1}$$

where we have defined the charging energy $E_C = \frac{(2e)^2}{2(C_g+2C_j)} \simeq 20E_J$, the gate-charge bias $N_g = \frac{C_g V_g}{(2e)}$, and the constant phase $0 \leqslant \theta_{ex} = \frac{\pi\Phi_{ex}}{\Phi_0} \leqslant \frac{\pi}{2}$ with the flux quantum $\Phi_0 = \frac{\pi\hbar}{e}$. We have also used the quantization

$$\hat{\phi} = \Phi_r(\hat{a}^\dagger + \hat{a}), \tag{2a}$$

$$\hat{Q} = iQ_r(\hat{a}^\dagger - \hat{a}), \tag{2b}$$

with the flux and charge constants

$$\Phi_r = \left(\frac{\hbar}{2}\sqrt{\frac{L}{C}}\right)^{1/2}, \tag{3a}$$

$$Q_r = \left(\frac{\hbar}{2}\sqrt{\frac{C}{L}}\right)^{1/2}. \tag{3b}$$

$\hat{a}^\dagger$ and $\hat{a}$ are the creation and annihilation microwave-photon operators. The phase θ_L is given by

$$\theta_L = \pi\xi\Phi_r/\Phi_0. \tag{4}$$

The system operates in the charging limit ($E_C \gg E_J$). We choose the basis $\{|n_c\rangle \otimes |n_p\rangle, n_c = 0, 1, 2, \ldots; n_p = 0, 1, 2, \ldots\}$, where n_c denotes the number of excess Cooper pairs in the box while n_p corresponds to the intraresonator photon number, to span the Hilbert space. The matrix elements of different operators are given by

$$\hat{N} = \sum_{n_c} n_c|n_c\rangle\langle n_c|, \tag{5a}$$

$$\cos\hat{\delta} = \sum_{n_c}(|n_c\rangle\langle n_c+1| + |n_c+1\rangle\langle n_c|), \tag{5b}$$

$$\hat{a} = \sum_{n_p}\sqrt{n_p}|n_p-1\rangle\langle n_p|. \tag{5c}$$

The αth eigenvalue $\mathcal{E}_\alpha$ and eigenstate Ψ_α of the system's Hamiltonian $\hat{H}$,

$$\hat{H}\Psi_\alpha = \mathcal{E}_\alpha\Psi_\alpha, \tag{6}$$

can be derived via the diagonalization method. Figure 1(b) displays $\mathcal{E}_{\alpha=1,\ldots,5}$ vs N_g for different θ_{ex} with $\xi = 1$. It is seen that a number of energy-level avoided crossings occur at the resonant multiphoton interaction. When $\theta_{ex} = 0$, a Cooper pair tunneling into (out of) the box leads to the decrement (increment) of the resonator field by $2k$ ($k \in \mathbb{Z}$) photons. For example, the anticrossing, which is labeled as A_2 and localized at $N_g^{(A_2)} = \frac{1}{2} - \frac{\hbar\omega_0}{E_C} = 0.38$, has a gap of $\hbar\Omega_{A_2} = 0.51E_J$ and occurs between two curves associated with $|n_c = 1\rangle \otimes |n_p = 0\rangle$ and $|n_c = 0\rangle \otimes |n_p = 2\rangle$ at $N_g = 0$. This is because the operator

$$\cos[\theta_L(\hat{a}^\dagger + \hat{a})] = \sum_j \frac{\theta_L^{2j}}{(2j)!}(\hat{a}^\dagger + \hat{a})^{2j} \tag{7}$$

only causes the even-photon transition of the resonator field. In contrast, when $\theta_{ex} = \frac{\pi}{2}$ the photon number varies by $(2k + 1)$ for one unit change in the number of Cooper pairs inside the box since the operator

$$\sin[\theta_L(\hat{a}^\dagger + \hat{a})] = \sum_j \frac{\theta_L^{2j+1}}{(2j+1)!}(\hat{a}^\dagger + \hat{a})^{2j+1} \tag{8}$$

causes the odd-photon transition. For instance, the anticrossings A_1 and A_3 occur at $N_g^{(A_1)} = \frac{1}{2} - \frac{\hbar\omega_0}{2E_C} = 0.44$ and $N_g^{(A_3)} = \frac{1}{2} - \frac{3\hbar\omega_0}{2E_C} = 0.33$ and have energy gaps of $\hbar\Omega_{A_1} = 0.57E_J$ and $\hbar\Omega_{A_3} = 0.37E_J$.

In the following, we focus on the charge qubit formed by $|n_c = 0\rangle$ and $|n_c = 1\rangle$ states interacting with the resonator. N_g is restricted within the range from zero to 0.5. The operators $\hat{N}$ and $\cos\hat{\delta}$ may be rewritten as

$$\hat{N} = (1 + \hat{\sigma}_z)/2, \tag{9a}$$

$$\cos\hat{\delta} = (\hat{\sigma}_-^\dagger + \hat{\sigma}_-)/2, \tag{9b}$$

with the definitions

$$\hat{\sigma}_z = |n_c = 1\rangle\langle n_c = 1| - |n_c = 0\rangle\langle n_c = 0|, \tag{10a}$$

$$\hat{\sigma}_- = |n_c = 0\rangle\langle n_c = 1|. \tag{10b}$$

The physical model described in Fig. 1(a) is similar to the fluxonium-resonator system experimentally demonstrated in Refs. [22,23]. Although in both cases the qubit is inductively coupled to the resonator, they have distinct differences:

(i) Unlike the fluxonium qubit, our superconducting qubit operates in the charge limit.

(ii) In our system, the flux portion $\xi\hat{\phi}$ passes through both the Cooper-pair-box loop and the inductor L, and the qubit-resonator coupling strength depends on their geometric position. In contrast, the strong coupling between fluxonium and the resonator is implemented by employing the kinetic inductance of several Josephson junctions which are shared by both subcircuits [24].

(iii) The nonlinear fluxonium-resonator interaction component is strongly suppressed in the highly anharmonic regime. However, in our scheme the nonlinear coupling term plays the main role.

Taking into consideration the dissipation effect, the whole system is described by the following master equation [25]:

$$\frac{d}{dt}\hat{\rho} = \frac{1}{i\hbar}[\hat{H}, \hat{\rho}] + \gamma_{-}\mathcal{D}[\hat{\sigma}_{-}]\hat{\rho} + \frac{\gamma_{\varphi}}{2}\mathcal{D}[\hat{\sigma}_{z}]\hat{\rho} + \kappa\mathcal{D}[\hat{a}]\hat{\rho}, \tag{11}$$

where $\hat{\rho}$ is the density operator of the system and we have defined the energy-relaxation and dephasing rates $\gamma_{-} = 2\pi \times 0.06$ GHz and $\gamma_{\varphi} = 2\pi \times 0.13$ GHz of the charge qubit [4] and the Lindblad superoperator

$$\mathcal{D}[\hat{o}]\hat{\rho} = \hat{o}\hat{\rho}\hat{o}^{\dagger} - \tfrac{1}{2}\hat{o}^{\dagger}\hat{o}\hat{\rho} - \tfrac{1}{2}\hat{\rho}\hat{o}^{\dagger}\hat{o}. \tag{12}$$

κ denotes the photon decay rate and relies on the resonator's quality factor Q, i.e., $\kappa = \frac{\omega_0}{Q}$. Typically, Q varies from 10^3 to 10^7 [1], depending on the specific geometric structure of the resonator, and we have $\kappa \ll \gamma_{-}, \gamma_{\varphi}$.

III. FOCK-STATE MASER

The interface between a two-level atom and a high-Q cavity has been proven to be an ideal platform for realizing the fragile Fock-state radiation via state-reduction [26] and trapping-state [27,28] schemes. Recently, Fock states with up to six photons have been also experimentally demonstrated based on a superconducting quantum circuit where a solid-state qubit acts as an intermediary between classical microwave pulses and the quantum resonator field [29,30]. Those methods all rely on the single-photon (artificial)-atom–resonator interaction. Here we present an alternative way to produce the number-state microwave field by utilizing the resonant multiphoton artificial-atom–resonator coupling.

As an example, we focus on the generation of an $|n_p = 1, 2, 3\rangle$ resonator field under the pulsed operation. The specific implementation is summarized as follows:

(i) The system is initially prepared in $|n_c = 1\rangle \otimes |n_p = 0\rangle$ and the gate-charge bias N_g is set at zero. The charge qubit barely interacts with the resonator due to the large detuning at $N_g = 0$.

(ii) Then, N_g nonadiabatically goes up to $N_g^{(A_{i=1,2,3})}$, where the avoided crossing $A_{i=1,2,3}$ occurs [see Fig. 1(b)], via tuning the voltage source V_g. The anticrossing starts the resonant single- or multiphoton ($|n_c = 1\rangle \otimes |n_p = 0\rangle - |n_c = 0\rangle \otimes |n_p = 1, 2, 3\rangle$) transition.

(iii) After a time duration τ, N_g is rapidly ramped back to zero so as to turn off the qubit-resonator interaction. Indeed, the system works as a pulsed maser, where the artificial qubit plays the gain-medium role.

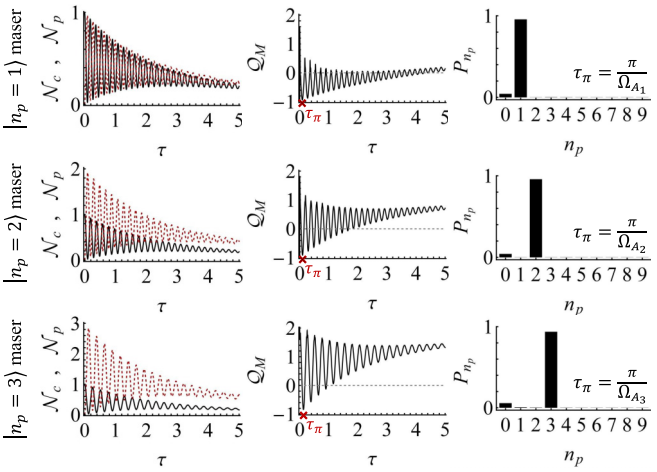

FIG. 2. Fock-state maser with $|n_p = 1, 2, 3\rangle$. Left: Charge-qubit excitation $\mathcal{N}_c$ (solid) and intraresonator photon number $\mathcal{N}_p$ (dashed line) vs pulse length τ. Middle: Dependence of Mandel $\mathcal{Q}_M$ parameter (solid line) on τ. The dashed line corresponds to $\mathcal{Q}_M = 0$. Right: Photon distribution P_{n_p} at $\tau_\pi = \frac{\pi}{\Omega_{A_{i=1,2,3}}}$. For all curves, $\xi = 1$ and $Q = 5 \times 10^3$ which gives $\kappa = 2\pi \times 4.5$ MHz.

Solving Eq. (11) gives us the charge-qubit excitation

$$\mathcal{N}_c = \mathrm{Tr}(\hat{\rho}\hat{N}), \tag{13}$$

and the intraresonator photon number

$$\mathcal{N}_p = \mathrm{Tr}(\hat{\rho}\hat{a}^{\dagger}\hat{a}), \tag{14}$$

at the end of ramp pulse. Figure 2 depicts the dependence of $\mathcal{N}_{c,p}$ on the pulse length τ. It is seen that the Rabi oscillation of the maser between $|n_p = 0\rangle$ and $|n_p = 1, 2, 3\rangle$ is strongly damped because of large γ_{-} and γ_{φ}. The Mandel parameter

$$\mathcal{Q}_M = \frac{\mathrm{Tr}(\hat{\rho}\hat{a}^{\dagger}\hat{a}\hat{a}^{\dagger}\hat{a}) - \mathcal{N}_p^2}{\mathcal{N}_p} \tag{15}$$

is commonly employed to measure the departure of a radiation from the classical field. $\mathcal{Q}_M < 0$ corresponds to a sub-Poissonian (nonclassical) photon-number statistics and $\mathcal{Q}_M$ arrives at -1 for Fock states. As illustrated in Fig. 2, $\mathcal{Q}_M$ minimizes at the π-pulse length $\tau_\pi = \frac{\pi}{\Omega_{A_{i=1,2,3}}}$. However, due to the charge qubit's relaxation, $\mathcal{Q}_M$ does not reach -1. Nevertheless, at τ_π the photon distribution $P_{n_p} = \langle n_p|\mathrm{Tr}_c(\hat{\rho})|n_p\rangle$ of the maser field, where Tr_c denotes the trace over the charge-qubit coordinates, is maximized at the corresponding Fock state with a probability greater than 90%. Thus, the production of a Fock-state pulsed maser requires the ramp-pulse length $\tau = \tau_\pi$. The lifetime of the Fock-state field is limited by κ^{-1}. The approach used here to produce multiphoton Fock-state radiation is applicable to arbitrary photon numbers up to $n_p^{\max} = \frac{E_C}{\hbar\omega_0} \simeq 8$, higher than which the populations in $|n_c = 1\rangle \otimes |n_p \neq 0\rangle$ rise and the fidelity of Fock-state generation degrades.

IV. RADIATION SQUEEZING

The nonlinear qubit-resonator interface may be also applied to generate the squeezed resonator field. In general, the

two-photon parametric process has been envisaged as a source of squeezing the radiation, for which we set $\theta_{ex} = 0$. Furthermore in the weak-coupling limit ($\theta_L \sim 0$ with $\xi \sim 0$), we approximate $\cos[\theta_L(\hat{a}^\dagger + \hat{a})]$ with the Taylor-series expansion of θ_L up to second order,

$$\cos[\theta_L(\hat{a}^\dagger + \hat{a})] \simeq 1 - \frac{\theta_L^2}{2}(\hat{a}^\dagger + \hat{a})^2. \tag{16}$$

Thus, the Hamiltonian is simplified as $\hat{H} \simeq \hat{H}_c + \hat{H}_p$ with the free charge-qubit Hamiltonian

$$\hat{H}_c = E_C\left(\frac{1}{2} - N_g\right)\hat{\sigma}_z - \frac{E_J}{2}(\hat{\sigma}_-^\dagger + \hat{\sigma}_-), \tag{17}$$

and the Hamiltonian associated with the resonator field,

$$\hat{H}_p = \hbar\omega_0 \hat{a}^\dagger \hat{a} + \frac{\theta_L^2 E_J}{4}(\hat{a}^\dagger + \hat{a})^2(\hat{\sigma}_-^\dagger + \hat{\sigma}_-). \tag{18}$$

To resonantly drive the two-photon transition, we sweep N_g periodically around $N_g^{(A_2)}$ with an amplitude $\Delta N_g = \frac{\hbar\Omega}{2E_C}$ ($\Omega \ll \omega_0$) and a rate $2\omega_0$. Hence, we have $E_C(\frac{1}{2} - N_g) = 2\hbar\omega_0 + \hbar\Omega\cos 2\omega_0 t$. It is unpractical to numerically simulate the time evolution of the whole system directly based on the master equation (11). As we see below, in the adiabatic limit the charge-qubit and resonator-field dynamics can be approximately treated separately, much simplifying the calculation.

Due to $\kappa \ll \gamma_-, \gamma_\varphi$, the charge qubit arrives at the quasisteady state much faster than the resonator field. In addition, the reaction of the qubit-resonator coupling on the charge-qubit dynamics is weak because of $\theta_L^2 \sim 0$. Thus, in the adiabatic approximation [31] we consider the dissipative time evolution of the charge qubit separately, which is governed by the following master equation:

$$\frac{d}{dt}\hat{\rho}^{(c)} = \frac{1}{i\hbar}[\hat{H}_c, \hat{\rho}^{(c)}] + \gamma_-\mathcal{D}[\hat{\sigma}_-]\hat{\rho}^{(c)} + \frac{\gamma_\varphi}{2}\mathcal{D}[\hat{\sigma}_z]\hat{\rho}^{(c)}, \tag{19}$$

where $\hat{\rho}^{(c)}$ is the charge-qubit density matrix operator. Equation (19) gives us

$$\frac{d}{dt}\rho_{11}^{(c)} = -\gamma_-\rho_{11}^{(c)} + i\frac{E_J}{2\hbar}\left[(\rho_{10}^{(c)})^* - \rho_{10}^{(c)}\right], \tag{20a}$$

$$\frac{d}{dt}\rho_{10}^{(c)} = \left(-\frac{\gamma_-}{2} - \gamma_\varphi - i2\omega_0 - i\Omega\cos 2\omega_0 t\right)\rho_{10}^{(c)} + i\frac{E_J}{2\hbar}\left(1 - 2\rho_{11}^{(c)}\right), \tag{20b}$$

with $\rho_{uv}^{(c)} = \langle n_c = u|\hat{\rho}^{(c)}|n_c = v\rangle$ $(u, v = 0, 1)$. Substituting $\rho_{10}^{(c)} = \tilde{\rho}_{10}^{(c)} e^{-i2\omega_0 t - i\frac{\Omega}{2\omega_0}\sin 2\omega_0 t}$ into the above two equations and applying the rotating-wave approximation (RWA), we arrive at

$$\frac{d}{dt}\rho_{11}^{(c)} \simeq -\gamma_-\rho_{11}^{(c)} - i\frac{\Omega}{2\omega_0}\frac{E_J}{4\hbar}\left[(\tilde{\rho}_{10}^{(c)})^* - \tilde{\rho}_{10}^{(c)}\right], \tag{21a}$$

$$\frac{d}{dt}\tilde{\rho}_{10}^{(c)} \simeq \left(-\frac{\gamma_-}{2} - \gamma_\varphi\right)\tilde{\rho}_{10}^{(c)} - i\frac{\Omega}{2\omega_0}\frac{E_J}{4\hbar}\left(1 - 2\rho_{11}^{(c)}\right). \tag{21b}$$

The steady-state (ss) solutions are derived as

$$\rho_{11}^{(c,ss)} = 2\lambda, \tag{22a}$$

$$\tilde{\rho}_{10}^{(c,ss)} = -i\lambda, \tag{22b}$$

with the parameter

$$\lambda = \gamma_-\left(\frac{\Omega}{2\omega_0}\frac{E_J}{4\hbar}\right)\Big/\left[\gamma_-\left(\frac{\gamma_-}{2} + \gamma_\varphi\right) + 4\left(\frac{\Omega}{2\omega_0}\frac{E_J}{4\hbar}\right)^2\right]. \tag{23}$$

In the limit of $\Omega \ll (2\omega_0)$, we have $\lambda \ll 1$ and the charge qubit is mostly populated in the ground state $|n_c = 0\rangle$.

Since the charge qubit is in the quasisteady state, we replace $\hat{\sigma}_-$ in $\hat{H}_p$ by $\tilde{\rho}_{10}^{(c,ss)} e^{-i2\omega_0 t - i\frac{\Omega}{2\omega_0}\sin 2\omega_0 t}$. Using the master equation for the resonator-field density matrix operator $\hat{\rho}^{(p)}$,

$$\frac{d}{dt}\hat{\rho}^{(p)} = \frac{1}{i\hbar}[\hat{H}_p, \hat{\rho}^{(p)}] + \kappa\mathcal{D}[\hat{a}]\hat{\rho}^{(p)}, \tag{24}$$

one obtains

$$\frac{d}{dt}\mathcal{A} = \left(-\frac{\kappa}{2} - i\omega_0\right)\mathcal{A} + i\lambda\theta_L^2\frac{E_J}{\hbar}(\mathcal{A}^* + \mathcal{A})\sin 2\omega_0 t, \tag{25a}$$

$$\frac{d}{dt}\mathcal{B} = \left(-\kappa - i2\omega_0 + i2\lambda\theta_L^2\frac{E_J}{\hbar}\sin 2\omega_0 t\right)\mathcal{B} + i\lambda\theta_L^2\frac{E_J}{\hbar}(2\mathcal{N}_p + 1)\sin 2\omega_0 t, \tag{25b}$$

$$\frac{d}{dt}\mathcal{N}_p = -\kappa\mathcal{N}_p + i\lambda\theta_L^2\frac{E_J}{\hbar}(\mathcal{B}^* - \mathcal{B})\sin 2\omega_0 t. \tag{25c}$$

Here we have defined $\mathcal{A} = \mathrm{Tr}(\hat{\rho}^{(p)}\hat{a})$ and $\mathcal{B} = \mathrm{Tr}(\hat{\rho}^{(p)}\hat{a}\hat{a})$ and used $\mathcal{N}_p = \mathrm{Tr}(\hat{\rho}^{(p)}\hat{a}^\dagger\hat{a})$. Substituting $\mathcal{A} = \tilde{\mathcal{A}}e^{-i\omega_0 t}$ and $\mathcal{B} = \tilde{\mathcal{B}}e^{-i2\omega_0 t - i\frac{\lambda\theta_L^2 E_J}{\hbar\omega_0}\cos 2\omega_0 t}$ into the above equations and applying the RWA, we arrive at

$$\frac{d}{dt}\tilde{\mathcal{A}} \simeq -\frac{\kappa}{2}\tilde{\mathcal{A}} - \frac{\lambda\theta_L^2}{2}\frac{E_J}{\hbar}\tilde{\mathcal{A}}^*, \tag{26a}$$

$$\frac{d}{dt}\tilde{\mathcal{B}} \simeq -\kappa\tilde{\mathcal{B}} - \frac{\lambda\theta_L^2}{2}\frac{E_J}{\hbar}(2\mathcal{N}_p + 1),$$

$$\frac{d}{dt}\mathcal{N}_p \simeq -\kappa\mathcal{N}_p - \frac{\lambda\theta_L^2}{2}\frac{E_J}{\hbar}(\tilde{\mathcal{B}}^* + \tilde{\mathcal{B}}). \tag{26b}$$

The steady-state solutions are then given by

$$\tilde{\mathcal{A}}^{(ss)} = 0, \tag{27a}$$

$$\tilde{\mathcal{B}}^{(ss)} = -\frac{\mu}{2}\frac{1}{1-\mu^2}, \tag{27b}$$

$$\mathcal{N}_p^{(ss)} = \frac{1}{2}\frac{\mu^2}{1-\mu^2}, \tag{27c}$$

with the parameter

$$\mu = \frac{\lambda\theta_L^2 E_J}{\hbar\kappa}. \tag{28}$$

Despite $\lambda \ll 1$ and $\theta_L \sim 0$, reducing κ may enhance μ. As μ approaches unity, the intraresonator photon number $\mathcal{N}_p^{(ss)}$ is strongly increased. However, the charge-qubit picture becomes invalid when $\mathcal{N}_p^{(ss)} > n_p^{\max}$ since the number of excess Cooper pairs in the box exceeds unity. Thus, the maximum of μ is given by $\mu^{\max} = \sqrt{\frac{2n_p^{\max}}{1+2n_p^{\max}}} \simeq 0.97$, leading to the required $\kappa = 2\pi \times 0.1$ MHz with the achievable quality factor $Q \sim 10^5$.

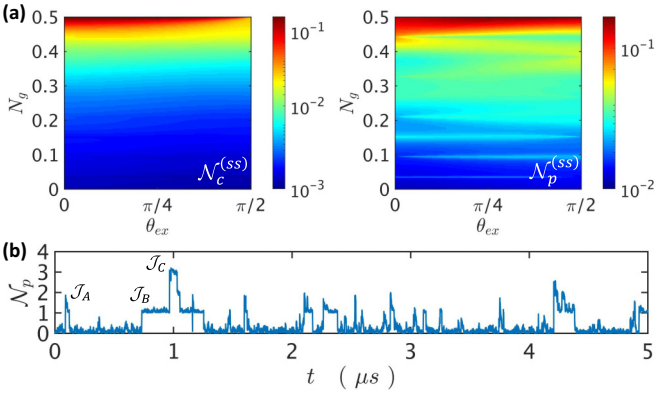

FIG. 3. (a) Steady-state $\mathcal{N}_{c,p}^{(ss)}$ as a function of N_g and θ_{ex}. (b) Trajectory of photon-number expectation value $\mathcal{N}_p$ with $N_g = \frac{1}{2}$ and $\theta_{ex} = 0$. The system is initially prepared in $|n_c = 0\rangle \otimes |n_p = 0\rangle$. All system parameters are same as in Fig. 2.

We then define two quadrature operators

$$\hat{X}_1 = \frac{1}{2}(\hat{a}e^{i\omega_0 t} + \hat{a}^\dagger e^{-i\omega_0 t}), \tag{29a}$$

$$\hat{X}_2 = \frac{1}{2i}(\hat{a}e^{i\omega_0 t} - \hat{a}^\dagger e^{-i\omega_0 t}), \tag{29b}$$

for the resonator field. In the steady state, the variances

$$\Delta X_{i=1,2}^{(ss)} = \sqrt{\langle \hat{X}_i^2 \rangle^{(ss)} - (\langle \hat{X}_i \rangle^{(ss)})^2} \tag{30}$$

are derived as $\Delta X_1^{(ss)} \simeq \frac{1}{2\sqrt{1+u}}$ and $\Delta X_2^{(ss)} \simeq \frac{1}{2\sqrt{1-u}}$. The best squeezing is achieved when $\mu = \mu^{\max}$, i.e., $\Delta X_1^{(ss)} \simeq \frac{1}{2\sqrt{1+\mu^{\max}}} = 0.36$. Further reducing $\Delta X_1^{(ss)}$ requires a larger $n_p^{\max}$ (i.e., a larger E_C and a smaller ω_0) and a smaller κ (i.e., a higher Q).

V. MULTIPHOTON QUANTUM JUMPS

The nonlinear interacting system may arrive at a nontrivial steady state ($\mathcal{N}_{c,p}^{(ss)} \neq 0$) even without an external driving. Setting $\frac{d}{dt}\hat{\rho} = 0$ in Eq. (11), one can derive the steady-state density matrix, i.e., $\hat{\rho}(t \to \infty)$, by employing the diagonalization approach [32]. The results are shown in Fig. 3(a). It is seen that both $\mathcal{N}_c^{(ss)}$ and $\mathcal{N}_p^{(ss)}$ are maximized at the sweet spot $N_g = 0.5$ because the Cooper-pair tunneling resonantly pumps the qubit from $|0\rangle$ to $|1\rangle$. In addition, due to $E_J \sim \hbar\omega_0$, the qubit-resonator interaction reaches the ultrastrong-coupling regime and the counter-rotating terms also play an important role in the intraresonator power enhancement.

We further employ the Monte Carlo wave-function method [33] to look into more detail about the dissipative artificial-atom–photon interaction in the steady state. Figure 3(b) illustrates a quantum trajectory corresponding to the time evolution of the photon-number expectation value $\mathcal{N}_p$ at $N_g = \frac{1}{2}$ and $\theta_{ex} = 0$. As one can see, multiple quantum jumps are presented and most of them are from the charge-qubit spontaneous decaying because of $\kappa \ll \gamma_-, \gamma_\varphi$. Such quantum-jump dynamics have been experimentally observed in macroscopic superconducting systems [34–36].

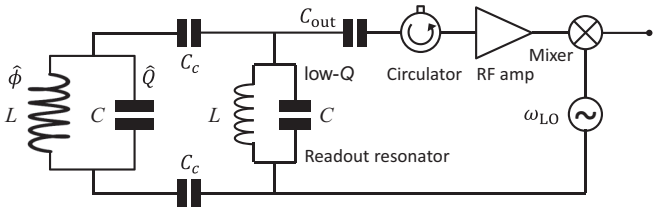

FIG. 4. QND measurement. The low-Q readout resonator, whose inductance and capacitance are equal to L and C, is weakly coupled with the LC resonator in the QED system via the coupling capacitors C_c. The inter-resonator coupling strength g is proportional to C_c, i.e., $g \propto (C_c/C)$, and the readout resonator barely affects the QED resonator in the limit $C_c \ll C$. The loss rate $\tilde{\kappa}$ of the readout resonator is much larger than κ and γ_-. The quantum trajectory $\mathcal{N}_p$ is mapped onto the intraresonator photon number $\tilde{\mathcal{N}}_p$ of the readout resonator, $\tilde{\mathcal{N}}_p \approx (g/\tilde{\kappa})^2\mathcal{N}_p$. $\tilde{\mathcal{N}}_p$ is measured via an output capacitor C_{out}, a circulator, a radio-frequency amplifier, and mixing with a local oscillator at ω_{LO} [14]. The circulator prevents leakage of thermal radiation into the resonator.

At any time, the system is in a superposition state completely composed of odd or even Fock states. After each photonic jump associated with the jump operator $\sqrt{\kappa}\hat{a}$, odd (even) Fock states transfer to lower even (odd) Fock states. Figure 3(b) clearly shows a number of sharp jumps with the photon-number differences of about one and two (or more than two). Some of them are induced by $\sqrt{\kappa}\hat{a}$ [e.g., the jumps $\mathcal{J}_{A,B}$ in Fig. 3(b)] while others are caused by the qubit decay associated with the jump operator $\sqrt{\gamma_-}\hat{\sigma}_-$ [e.g., the jump $\mathcal{J}_C$ in Fig. 3(b)]. We consider the trajectory period from $\mathcal{J}_A$ to $\mathcal{J}_C$. Before $\mathcal{J}_A$ occurs, the system is mainly in the vacuum $|n_p = 0\rangle$ state with the secondary-weighted component of $|n_p = 2\rangle$. Subsequently, the jump $\mathcal{J}_A$ collapses the system's wave function onto $|n_p = 1\rangle$. Similarly, at $\mathcal{J}_B$ the system collapses onto $|n_c = 0\rangle \otimes |n_p = 1\rangle$. Afterwards, the system evolves to a superposition state with a component of $|n_c = 1\rangle \otimes |n_p = 3\rangle$ via the counter-rotating parametric process (i.e., $\hat{\sigma}_-^\dagger \hat{a}^\dagger \hat{a}^\dagger$). Then, the jump operator $\sqrt{\gamma_-}\sigma_-$ collapses the system's wave function onto $|n_c = 0\rangle \otimes |n_p = 3\rangle$ at $\mathcal{J}_C$.

Observing quantum jumps of $\mathcal{N}_p$ relies on the quantum nondemolition (QND) measurement at a rate much faster than κ and γ_- [35]. Such a measurement may be performed, as an example, by weakly coupling the LC resonator with another resonator (called the readout resonator) whose inductance and capacitance are equal to L and C (see Fig. 4). The inter-resonator coupling strength g is small enough that the readout resonator barely affects the QED system. In addition, the Q factor of the readout resonator is very low, leading to a loss rate $\tilde{\kappa}$ much larger than κ and γ_-. Thus, the readout-resonator field always follows the one in the QED circuit adiabatically. The intraresonator photon number $\tilde{\mathcal{N}}_p$ of the readout resonator approximates $\tilde{\mathcal{N}}_p \approx (g/\tilde{\kappa})^2\mathcal{N}_p$. Consequently, quantum jumps can be observed by measuring $\tilde{\mathcal{N}}_p$.

VI. CONCLUSION

We have studied a nonlinear circuit-QED scheme where a charge qubit is inductively coupled to a microwave resonator via multiphoton processes. Such an architecture can produce

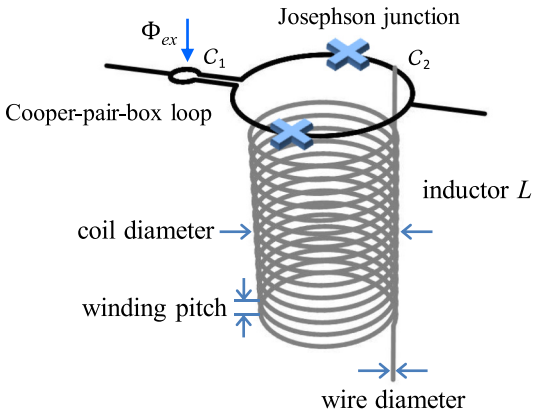

FIG. 5. Nonlinear inductive qubit-resonator coupling. The resonator's inductor L is in the single-layer vacuum-core solenoid structure. The Cooper-pair-box loop of the charge qubit presents two circles separated far enough from each other. The external flux Φ_{ex} goes through one circle while the flux portion $\xi\hat{\phi}$ from L threads the other circle.

arbitrary photon-number states of a resonator field with a high fidelity, which is of particular importance for linear photonic quantum computing [37,38]. The squeezed radiation may be generated by the parametric qubit-resonator interface, potentially applicable to the quantum-limited microwave amplifier [39]. This platform can also be employed to investigate fundamental principles of multiphoton light-matter interaction in the ultrastrong-coupling regime [40], where, as we have illustrated, the counter-rotating terms and qubit decay jointly lead to upwards multiphoton quantum jumps of the resonator field. The rapid development of cryogenic electronics may sustain much longer lifetimes of superconducting circuits in the future, enabling more potential applications of circuit QED in quantum information processing and fundamental new physics.

ACKNOWLEDGMENTS

This research has been supported by the National Research Foundation Singapore and by the Ministry of Education Singapore Academic Research Fund Tier 2 (Grant No. MOE2015-T2-1-101).

APPENDIX: PARAMETER ξ

The physical scheme described in Fig. 1(a) has various implementations in experiment. Here we show in principle that the parameter ξ, which measures the qubit-resonator coupling, may be tuned between zero and 1.

We take the single-layer vacuum-core solenoid as an example to form the resonator's inductor L (see Fig. 5). Based on the Wheeler formula for the inductance calculation [41,42], the specific structure of L can be chosen as the coil diameter of 50 μm, the wire diameter of 5 μm, the winding pitch of 6 μm, and the number of turns, 250, resulting in $L = 100$ nH. According to [43], the stray capacitance of L is estimated to be less than 30 aF, much smaller than the resonator's capacitor C. This tiny parasitic capacitance is connected in parallel with L in the equivalent circuit model [44] and its effect on the circuit is negligible. We should note that the design of L has other options, such as the planar spiral structure [45].

As shown in Fig. 5, the Cooper-pair-box loop consists of two circles, $\mathcal{C}_1$ and $\mathcal{C}_2$, which are far apart from each other. The external flux Φ_{ex} mainly passes through $\mathcal{C}_1$ while the flux portion $\xi\hat{\phi}$ from L primarily threads the circle $\mathcal{C}_2$. The inductor L is aligned perpendicular to the plane of $\mathcal{C}_2$. The area of $\mathcal{C}_2$ is similar to the coil area of L. The parameter ξ can be tuned by adjusting the relative position between the Cooper-pair-box loop and L along the vertical direction. When L completely penetrates the circle $\mathcal{C}_2$, we obtain the maximum $\xi = 1$. As L moves away from $\mathcal{C}_2$ vertically, ξ goes down.

[1] Z.-L. Xiang, S. Ashhab, J. Q. You, and F. Nori, Rev. Mod. Phys. **85**, 623 (2013).
[2] C. Wang, Y. Y. Gao, P. Reinhold, R. W. Heeres, N. Ofek, K. Chou, C. Axline, M. Reagor, J. Blumoff, K. M. Sliwa, L. Frunzio, S. M. Girvin, L. Jiang, M. Mirrahimi, M. H. Devoret, and R. J. Schoelkopf, Science **352**, 1087 (2016).
[3] R. Vijay, C. Macklin, D. H. Slichter, S. J. Weber, K. W. Murch, R. Naik, A. N. Korotkov, and I. Siddiqi, Nature (London) **490**, 77 (2012).
[4] D. Yu, A. Landra, L. C. Kwek, L. Amico, and R. Dumke, New J. Phys. **20**, 023031 (2018).
[5] D. Yu and R. Dumke, Phys. Rev. A **97**, 053813 (2018).
[6] D. Yu, M. M. Valado, C. Hufnagel, L. C. Kwek, L. Amico, and R. Dumke, Phys. Rev. A **93**, 042329 (2016).
[7] D. Yu, A. Landra, M. M. Valado, C. Hufnagel, L. C. Kwek, L. Amico, and R. Dumke, Phys. Rev. A **94**, 062301 (2016).
[8] D. Yu, M. M. Valado, C. Hufnagel, L. C. Kwek, L. Amico, and R. Dumke, Sci. Rep. **6**, 38356 (2016).
[9] D. Yu, L. C. Kwek, L. Amico, and R. Dumke, Quantum Sci. Technol. **2**, 035005 (2017).
[10] C. Hufnagel, A. Landra, L. C. Chean, D. Yu, and R. Dumke, Proc. SPIE **10358**, 1035801 (2017).
[11] T. Niemczyk, F. Deppe, H. Huebl, E. P. Menzel, F. Hocke, M. J. Schwarz, J. J. Garcia-Ripoll, D. Zueco, T. Hümmer, E. Solano, A. Marx, and R. Gross, Nat. Phys. **6**, 772 (2010).
[12] F. Yoshihara, T. Fuse, S. Ashhab, K. Kakuyanagi, S. Saito, and K. Semba, Nat. Phys. **13**, 44 (2017).
[13] D. Yu, L. C. Kwek, L. Amico, and R. Dumke, Phys. Rev. A **95**, 053811 (2017).
[14] A. Wallraff, D. I. Schuster, A. Blais, L. Frunzio, R.-S. Huang, J. Majer, S. Kumar, S. M. Girvin, and R. J. Schoelkopf, Nature (London) **431**, 162 (2004).
[15] A. Blais, R.-S. Huang, A. Wallraff, S. M. Girvin, and R. J. Schoelkopf, Phys. Rev. A **69**, 062320 (2004).
[16] K. Xu, J.-J. Chen, Y. Zeng, Y.-R. Zhang, C. Song, W. Liu, Q. Guo, P. Zhang, D. Xu, H. Deng, K. Huang, H. Wang, X. Zhu, D. Zheng, and H. Fan, Phys. Rev. Lett. **120**, 050507 (2018).
[17] A. A. Houck, H. E. Türeci, and J. Koch, Nat. Phys. **8**, 292 (2012).

[18] T. Yamamoto, K. Inomata, M. Watanabe, K. Matsuba, T. Miyazaki, W. D. Oliver, Y. Nakamura, and J. S. Tsai, Appl. Phys. Lett. **93**, 042510 (2008).
[19] J. Y. Mutus, T. C. White, R. Barends, Y. Chen, Z. Chen, B. Chiaro, A. Dunsworth, E. Jeffrey, J. Kelly, A. Megrant, C. Neill, P. J. J. O'Malley, P. Roushan, D. Sank, A. Vainsencher, J. Wenner, K. M. Sundqvist, A. N. Cleland, and J. M. Martinis, Appl. Phys. Lett. **104**, 263513 (2014).
[20] F. Dell'Anno, S. D. Siena, and F. Illuminati, Phys. Rep. **428**, 53 (2006).
[21] Y. Makhlin, G. Scöhn, and A. Shnirman, Nature (London) **398**, 305 (1999).
[22] I. M. Pop, K. Geerlings, G. Catelani, R. J. Schoelkopf, L. I. Glazman, and M. H. Devoret, Nature (London) **508**, 369 (2014).
[23] W. C. Smith, A. Kou, U. Vool, I. M. Pop, L. Frunzio, R. J. Schoelkopf, and M. H. Devoret, Phys. Rev. B **94**, 144507 (2016).
[24] V. E. Manucharyan, J. Koch, L. I. Glazman, and M. H. Devoret, Science **326**, 113 (2009).
[25] H. J. Carmichael, *An Open Systems Approach to Quantum Optics* (Springer-Verlag, New York, 1993).
[26] B. T. H. Varcoe, S. Brattke, M. Weidinger, and H. Walther, Nature (London) **403**, 743 (2000).
[27] P. Meystre, G. Rempe, and H. Walther, Opt. Lett. **13**, 1078 (1988).
[28] S. Brattke, B. T. H. Varcoe, and H. Walther, Phys. Rev. Lett. **86**, 3534 (2001).
[29] M. Hofheinz, E. M. Weig, M. Ansmann, R. C. Bialczak, E. Lucero, M. Neeley, A. D. O'Connell, H. Wang, J. M. Martinis, and A. N. Cleland, Nature (London) **454**, 310 (2008).
[30] H. Wang, M. Hofheinz, M. Ansmann, R. C. Bialczak, E. Lucero, M. Neeley, A. D. O'Connell, D. Sank, J. Wenner, A. N. Cleland, and John M. Martinis, Phys. Rev. Lett. **101**, 240401 (2008).
[31] M. O. Scully and M. S. Zubairy, *Quantum Optics* (Cambridge University Press, Cambridge, UK, 1997).
[32] D. Yu, J. Opt. Soc. Am. B **33**, 797 (2016).
[33] K. Mølmer, Y. Castin, and J. Dalibard, J. Opt. Soc. Am. B **10**, 524 (1993).
[34] Y. Yu, S. L. Zhu, G. Sun, X. Wen, N. Dong, J. Chen, P. Wu, and S. Han, Phys. Rev. Lett. **101**, 157001 (2008).
[35] R. Vijay, D. H. Slichter, and I. Siddiqi, Phys. Rev. Lett. **106**, 110502 (2011).
[36] U. Vool, I. M. Pop, K. Sliwa, B. Abdo, C. Wang, T. Brecht, Y. Y. Gao, S. Shankar, M. Hatridge, G. Catelani, M. Mirrahimi, L. Frunzio, R. J. Schoelkopf, L. I. Glazman, and M. H. Devoret, Phys. Rev. Lett. **113**, 247001 (2014).
[37] E. Knill, R. Laflamme, and G. J. Milburn, Nature (London) **409**, 46 (2001).
[38] P. Kok, W. J. Munro, K. Nemoto, T. C. Ralph, J. P. Dowling, and G. J. Milburn, Rev. Mod. Phys. **79**, 135 (2007).
[39] M. A. Castellanos-Beltran, K. D. Irwin, G. C. Hilton, L. R. Vale, and K. W. Lehnert, Nat. Phys. **4**, 929 (2008).
[40] L. Garziano, R. Stassi, V. Macrì, A. F. Kockum, S. Savasta, and F. Nori, Phys. Rev. A **92**, 063830 (2015).
[41] H. A. Wheeler, Proc. IRE **16**, 1398 (1928).
[42] H. A. Wheeler, Proc. IEEE **70**, 1449 (1982).
[43] G. Grandi, M. K. Kazimierczuk, A. Massarini, and U. Reggiani, IEEE Trans. Ind. Appl. **35**, 1162 (1999).
[44] H. W. Ott, *Noise Reduction Techniques in Electronic Systems*, 2nd ed. (Wiley, New York, 1988).
[45] B. Sarabi, P. Huang, and N. M. Zimmerman, arXiv:1702.02210.